Enhancement of second-harmonic generation in nonlinear nanolaminate metamaterials by nanophotonic resonances

Hui-Hsin Hsiao,[1,*] Aimi Abass,[2] Johannes Fischer,[3] Rasoul Alaee,[1] Andreas Wickberg,[3] Martin Wegener,[2,3] and Carsten Rockstuhl[1,2]

[1]*Institute of Theoretical Solid State Physics, Karlsruhe Institute of Technology (KIT), Wolfgang-Gaede-Str. 1, 76128 Karlsruhe, Germany*
[2]*Institute of Nanotechnology, Karlsruhe Institute of Technology (KIT), P.O. Box 3640, 76021 Karlsruhe, Germany*
[3]*Institute of Applied Physics, Karlsruhe Institute of Technology (KIT), 76128 Karlsruhe, Germany*
[*]*d96941018@ntu.edu.tw*

Abstract: Nanolaminate metamaterials recently attracted a lot of attention as a novel second-order nonlinear material that can be used in integrated photonic circuits. Here, we explore theoretically and numerically the opportunity to enhance the nonlinear response from such nanolaminates by exploiting Fano resonances supported in grating-coupled waveguides. The enhancement factor of the radiated second harmonic signal compared to a flat nanolaminate can reach values as large as 35 for gold gratings and even 7000 for MgF_2 gratings. For the MgF_2 grating, extremely high-Q Fano resonances are excited in such all-dielectric system that result in strong local fields in the nonlinear waveguide layer to boost the nonlinear conversion. A significant portion of the nonlinear signal is also strongly coupled to a dark waveguide mode, which remains guided in the nanolaminate. The strong excitation of a dark mode at the second harmonic frequency provides a viable method for utilizing second-order nonlinearities for light generation and manipulation in integrated photonic circuits.

OCIS codes: (050.1950) Diffraction gratings; (230.7370) Waveguides; (050.6624) Subwavelength structures; (190.4350) Nonlinear optics at surfaces; (190.2620) Harmonic generation and mixing; (130.3120) Integrated optics devices.

References and links

1. R. W. Boyd, *Nonlinear Optics* (Elsevier Science, 2008).
2. T.-D. Kim, J. Luo, J.-W. Ka, S. Hau, Y. Tian, Z. Shi, N. M. Tucker, S.-H. Jang, J.-W. Kang, and A. K.-Y. Jen, "Ultralarge and thermally stable electro-optic activities from Diels-Alder crosslinkable polymers containing binary chromophore systems," Adv. Mater. **18**(22), 3038–3042 (2006).
3. K. Yadav, C. L. Callender, C. W. Smelser, C. Ledderhof, C. Blanchetiere, S. Jacob, and J. Albert, "Giant enhancement of the second harmonic generation efficiency in poled multilayered silica glass structures," Opt. Express **19**(27), 26975–26983 (2011).
4. M. Zdanowicz, J. Harra, J. M. Mäkelä, E. Heinonen, T. Ning, M. Kauranen, and G. Genty, "Second-harmonic response of multilayer nanocomposites of silver-decorated nanoparticles and silica," Sci. Rep. **4**, 5745 (2014).
5. F. B. P. Niesler, N. Feth, S. Linden, and M. Wegener, "Second-harmonic optical spectroscopy on split-ring-resonator arrays," Opt. Lett. **36**(9), 1533–1535 (2011).
6. R. Czaplicki, H. Husu, R. Siikanen, J. Mäkitalo, M. Kauranen, J. Laukkanen, J. Lehtolahti, and M. Kuittinen, "Enhancement of second-harmonic generation from metal nanoparticles by passive elements," Phys. Rev. Lett. **110**(9), 093902 (2013).
7. L. Luo, I. Chatzakis, J. Wang, F. B. P. Niesler, M. Wegener, T. Koschny, and C. M. Soukoulis, "Broadband terahertz generation from metamaterials," Nat. Commun. **5**(3055), 3055 (2014).
8. M. Celebrano, X. Wu, M. Baselli, S. Großmann, P. Biagioni, A. Locatelli, C. De Angelis, G. Cerullo, R. Osellame, B. Hecht, L. Duò, F. Ciccacci, and M. Finazzi, "Mode matching in multiresonant plasmonic nanoantennas for enhanced second harmonic generation," Nat. Nanotechnol. **10**(5), 412–417 (2015).
9. J. Butet, P.-F. Brevet, and O. J. F. Martin, "Optical second harmonic generation in plasmonic nanostructures: From fundamental principles to advanced applications," ACS Nano **9**(11), 10545–10562 (2015).
10. J. Lee, M. Tymchenko, C. Argyropoulos, P.-Y. Chen, F. Lu, F. Demmerle, G. Boehm, M.-C. Amann, A. Alù, and M. A. Belkin, "Giant nonlinear response from plasmonic metasurfaces coupled to intersubband transitions," Nature **511**(7507), 65–69 (2014).

#261024 Received 11 Mar 2016; revised 19 Apr 2016; accepted 19 Apr 2016; published 25 Apr 2016

11. L. Alloatti, C. Kieninger, A. Froelich, M. Lauermann, T. Frenzel, K. Köhnle, W. Freude, J. Leuthold, M. Wegener, and C. Koos, "Second-order nonlinear optical metamaterials: ABC-type nanolaminates," Appl. Phys. Lett. **107**(12), 121903 (2015).
12. S. Clemmen, A. Hermans, E. Solano, J. Dendooven, K. Koskinen, M. Kauranen, E. Brainis, C. Detavernier, and R. Baets, "Atomic layer deposited second-order nonlinear optical metamaterial for back-end integration with CMOS-compatible nanophotonic circuitry," Opt. Lett. **40**(22), 5371–5374 (2015).
13. B. Corcoran, C. Monat, C. Grillet, D. J. Moss, B. J. Eggleton, T. P. White, L. O'Faolain, and T. F. Krauss, "Green light emission in silicon through slow-light enhanced third-harmonic generation in photonic-crystal waveguides," Nat. Photonics **3**(4), 206–210 (2009).
14. D. de Ceglia, G. D'Aguanno, N. Mattiucci, M. A. Vincenti, and M. Scalora, "Enhanced second-harmonic generation from resonant GaAs gratings," Opt. Lett. **36**(5), 704–706 (2011).
15. S. B. Hasan, C. Rockstuhl, T. Pertsch, and F. Lederer, "Second-order nonlinear frequency conversion processes in plasmonic slot waveguides," J. Opt. Soc. Am. B **29**(7), 1606–1611 (2012).
16. Y. Sun, Z. Zheng, J. Cheng, G. Sun, and G. Qiao, "Highly efficient second harmonic generation in hyperbolic metamaterial slot waveguides with large phase matching tolerance," Opt. Express **23**(5), 6370–6378 (2015).
17. A. Saari, G. Genty, M. Siltanen, P. Karvinen, P. Vahimaa, M. Kuittinen, and M. Kauranen, "Giant enhancement of second-harmonic generation in multiple diffraction orders from sub-wavelength resonant waveguide grating," Opt. Express **18**(12), 12298–12303 (2010).
18. T. Ning, H. Pietarinen, O. Hyvärinen, R. Kumar, T. Kaplas, M. Kauranen, and G. Genty, "Efficient second-harmonic generation in silicon nitride resonant waveguide gratings," Opt. Lett. **37**(20), 4269–4271 (2012).
19. J. H. Lin, C.-Y. Tseng, C.-T. Lee, J. F. Young, H.-C. Kan, and C. C. Hsu, "Strong guided mode resonant local field enhanced visible harmonic generation in an azo-polymer resonant waveguide grating," Opt. Express **22**(3), 2790–2797 (2014).
20. M. H. Luong, T. T. N. Nguyen, C. T. Nguyen, I. Ledoux-Rak, and N. D. Lai, "Study of all-polymer-based waveguide resonant gratings and their applications for optimization of second-harmonic generation," J. Phys. D Appl. Phys. **48**(36), 365302 (2015).
21. T. Utikal, T. Zentgraf, T. Paul, C. Rockstuhl, F. Lederer, M. Lippitz, and H. Giessen, "Towards the origin of the nonlinear response in hybrid plasmonic systems," Phys. Rev. Lett. **106**(13), 133901 (2011).
22. T. Ning, C. Tan, T. Niemi, M. Kauranen, and G. Genty, "Enhancement of second-harmonic generation from silicon nitride with gold gratings," Opt. Express **23**(24), 30695–30700 (2015).
23. S. G. Tikhodeev, A. L. Yablonskii, E. A. Muljarov, N. A. Gippius, and T. Ishihara, "Quasiguided modes and optical properties of photonic crystal slabs," Phys. Rev. B **66**(4), 045102 (2002).
24. J. Butet and O. J. F. Martin, "Evaluation of the nonlinear response of plasmonic metasurfaces: Miller's rule, nonlinear effective susceptibility method, and full-wave computation," J. Opt. Soc. Am. B **33**(2), A8–A15 (2016).
25. G. E. Arnaoutakis, J. Marques-Hueso, A. Ivaturi, S. Fischer, J. C. Goldschmidt, K. W. Krämer, and B. S. Richards, "Enhanced energy conversion of up-conversion solar cells by the integration of compound parabolic concentrating optics," Sol. Energy Mater. Sol. Cells **140**, 217–223 (2015).
26. S. B. Hasan, F. Lederer, and C. Rockstuhl, "Nonlinear plasmonic antennas," Mater. Today **17**(10), 478–485 (2014).
27. M. Mesch, B. Metzger, M. Hentschel, and H. Giessen, "Nonlinear plasmonic sensing," Nano Lett. (posted 6 April 2016, in press).
28. A. Taflove, *Computational Electrodynamics: The Finite-Difference Time-Domain Method*, 3rd ed. (Artech House, 2005).
29. C. Kieninger, *Effective Bulk Second-Order Nonlinearity in ABC-Type Nanolaminate Optical Metamaterials*, (Master thesis, Karlsruhe Institute of Technology, 2015).
30. E. D. Palik, *Handbook of Optical Constants of Solids* (Academic, 1985).
31. H. H. Li, "Refractive index of alkaline earth halides and its wavelength and temperature derivatives," J. Phys. Chem. Ref. Data **9**(1), 161–289 (1980).
32. I. H. Malitson, "Interspecimen comparison of the refractive index of fused silica," J. Opt. Soc. Am. **55**(10), 1205–1209 (1965).
33. M. A. Alsunaidi, H. M. Al-Mudhaffar, and H. M. Masoudi, "Vectorial FDTD technique for the analysis of optical second-harmonic generation," IEEE Photonics Technol. Lett. **21**(5), 310–312 (2009).
34. C. M. Reinke, A. Jafarpour, B. Momeni, M. Soltani, S. Khorasani, A. Adibi, Y. Xu, and R. K. Lee, "Nonlinear finite-difference time-domain method for the simulation of anisotropic, $\chi^{(2)}$, and $\chi^{(3)}$ optical effects," J. Lightwave Technol. **24**(1), 624–634 (2006).
35. M. Balasubrahmaniyam, T. Abhilash, A. R. Ganesan, and S. Kasiviswanathan, "Effective medium-based plasmonic waveguides for tailoring dispersion," IEEE Photonics Technol. Lett. **27**(18), 1965–1968 (2015).
36. B. Gallinet and O. J. F. Martin, "Influence of electromagnetic interactions on the line shape of plasmonic Fano resonances," ACS Nano **5**(11), 8999–9008 (2011).
37. R. Alaee, D. Lehr, R. Filter, F. Lederer, E.-B. Kley, C. Rockstuhl, and A. Tünnermann, "Scattering dark states in multiresonant concentric plasmonic nanorings," ACS Photonics **2**(8), 1085–1090 (2015).
38. B. Metzger, L. Gui, J. Fuchs, D. Floess, M. Hentschel, and H. Giessen, "Strong enhancement of second harmonic emission by plasmonic resonances at the second harmonic wavelength," Nano Lett. **15**(6), 3917–3922 (2015).
39. T. Zentgraf, S. Zhang, R. F. Oulton, and X. Zhang, "Ultranarrow coupling-induced transparency bands in hybrid plasmonic systems," Phys. Rev. B **80**(19), 195415 (2009).

#261024 Received 11 Mar 2016; revised 19 Apr 2016; accepted 19 Apr 2016; published 25 Apr 2016

40. B. Luk'yanchuk, N. I. Zheludev, S. A. Maier, N. J. Halas, P. Nordlander, H. Giessen, and C. T. Chong, "The Fano resonance in plasmonic nanostructures and metamaterials," Nat. Mater. **9**(9), 707–715 (2010).
41. J. Pomplun, S. Burger, L. Zschiedrich, and F. Schmidt, "Adaptive finite element method for simulation of optical nano structures," Phys. Status Solidi **244**(10), 3419–3434 (2007).
42. A. Abass, S. R.-K. Rodriguez, J. G. Rivas, and B. Maes, "Tailoring dispersion and eigenfield profiles of plasmonic surface lattice resonances," ACS Photonics **1**(1), 61–68 (2014).

1. Introduction

Second-order nonlinear optical metamaterials have attracted increasing attention in recent years due to the wide range of practical applications such as efficient frequency conversion, biochemical sensing, and optical switching and memories [1]. They derive their properties not just from the intrinsic nonlinear properties of the constituents but also from the geometrical structure of the material. Very often, periodic unit cells are considered, however, aperiodic structures are possible, too. Compared to bulk nonlinear crystals, nonlinear optical metamaterials provide new possibilities for the integration of nonlinear optical functionalities into nanophotonic chips. Several methods have been demonstrated to achieve large effective nonlinear susceptibilities such as poling in polymers [2], alternating stacking of germanium-doped and undoped poled-silica layers [3], and exploiting metallic nanostructures with non-centrosymmetric geometries [4–9]. Lee *et al*. [10] also utilized inter-subband transitions in multi-quantum well semiconductor heterostructures at infrared wavelengths.

Recently, Alloatti *et al*. [11] and Clemmen *et al*. [12] used atomic-layer deposition to fabricate non-centrosymmetric nanolaminates. These nanolaminates are composed of a sequence of layers from three centrosymmetric dielectric materials. In consequence, each individual material possesses only a surface second-order nonlinearity. However, by using many layers with a nanometric thickness, the emerging bulk material consists effectively of densely packed surfaces. By using a stack of three layers made from different materials in each unit cell, the macroscopic centrosymmetry is broken and the second-order surface nonlinearity can be harvested since it translates effectively to a bulk second-order nonlinearity. This approach is especially promising for on-chip nonlinear optics because it is compatible with state-of-art complementary metal-oxide-semiconductor (CMOS) technology as well as substantial degrees of freedom for substrate materials.

To further enhance the effective susceptibilities of such nanolaminates, nanooptical concepts can be used that cause strong local fields. Possible approaches rely on photonic crystals [13], gratings [14], slot waveguides [15, 16], resonant waveguide gratings [17–20], or hybrid plasmonic waveguides [21, 22]. In this paper, we theoretically study the linear and nonlinear optical responses for one-dimensional nanostrip gratings made of either gold (Au) or magnesium fluoride (MgF_2), respectively, buried inside a nanolaminate metamaterial. This material on its own already acts as a waveguide layer. The periodic corrugation in such hybrid structure enables the coupling of the external illumination with waveguide (dark) modes [23]. The resulting quasi-guided (leaky) modes exhibit Fano line shapes in the spectra, and their strong local fields in the nanolaminate waveguide layer can be used to enhance the second-harmonic generation (SHG). The characteristic of Fano resonances and their roles in affecting the magnitude and spectral position of SHG is systematically investigated. We analytically model the devices and also present results from nonlinear full-wave numerical calculations [24]. Combined, these results allow to comprehensively understand the optical properties of such advanced nonlinear nanolaminate structures.

2. Grating-coupled nanolaminates

A schematic view of the considered hybrid structure is shown in Fig. 1. The nanostrip grating has a period of p = 500 nm and a height of h = 30 nm and 60 nm for the Au and MgF_2 gratings,

#261024 Received 11 Mar 2016; revised 19 Apr 2016; accepted 19 Apr 2016; published 25 Apr 2016

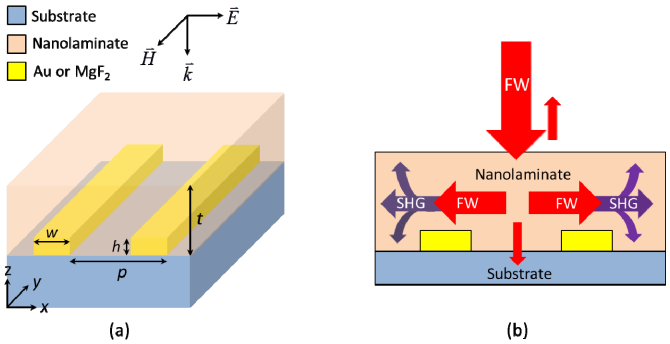

Fig. 1. (a) Scheme of the hybrid structure. The periodic nanostrips are embedded in the nanolaminate metamaterial with h = 30 nm for Au and h = 60 nm for MgF_2. (b) Illustration of the mechanism of the SHG enhancement in our structure. Light at the fundamental wavelength impinges onto the hybrid system and excites the quasi-guided mode in the nanolaminates (red-horizontal arrows). Transmitted and reflected partial waves as indicated by the downward- and upward-red arrows, respectively. The guided field interacts with the nonlinear medium and generates the SH signal.

respectively. The substrate is fused silica. The superstrate is air. The parameter we systematically change is the strip width w. Nonlinear nanolaminates with a thickness of 285.8 nm were considered accordingly as a waveguide layer. The scenario of the SHG enhancement is sketched in Fig. 1(b). First, the incoming fundamental wave (FW) is coupled to the quasi-guided mode and meanwhile amplifying the nonlinear conversion. The generated SH signal can be coupled to another waveguide mode, and also radiate to the air and glass substrate. Such normal-incident thin-film devices are promising to provide reasonable absolute second-harmonic generation efficiencies at visible frequencies in analogy to what has been presented in Ref. 10 at infrared wavelengths. Such materials constitute an excellent material plattform for multiple applications where high nonlinear conversion efficiencies are important, e.g. for the spectral conversion in light management devices where up- and down-conversion [25] is required or for nonlinear sensing devices [26, 27].

3. Numerical modelling

Full-wave electrodynamic calculations were performed with an in-house developed finite-difference time-domain (FDTD) program [28]. The optical data for nanolaminates were taken from ellipsometry measurements [29]. For Au, MgF_2, and the fused silica substrate, they were taken from literature values [30–32]. The dispersive permittivity for each material was fitted by a Drude-Lorentz model with two Lorentzian terms,

$$\varepsilon_r(\omega) = \varepsilon_\infty - \frac{\omega_d^2}{\omega^2 + i\gamma_d\omega} + \sum_{j=1}^{2} \frac{A_{Lj}\omega_{Lj}^2}{\omega_{Lj}^2 - i\gamma_{Lj}\omega - \omega^2}, \tag{1}$$

where ε_∞ is the high-frequency limit of the dielectric constant, ω_d and ω_{Lj} are the plasma frequencies, γ_d and γ_{Lj} are the effective damping rate, A_{Lj} is the weighting number of the j^{th} oscillator. The Drude-Lorentz model is then incorporated into the FDTD program by auxiliary differential equations [28]. Table 1 lists all the fitting parameters for the materials we concern. To calculate the SHG of the hybrid structure, the dispersive-FDTD is further extended to solve the nonlinear Maxwell's equations [1],

$$\nabla\times\vec{H}(\vec{r},t) = \varepsilon_0\varepsilon_\infty(\vec{r})\frac{\partial}{\partial t}\vec{E}(\vec{r},t) + \vec{J}_d(\vec{r},t) + \sum_i \vec{J}_{L_i}(\vec{r},t) + \frac{\partial}{\partial t}\vec{P}^{(2)}(\vec{r},t) \tag{2}$$

$$\vec{P}^{(2)}(\vec{r},t) = \varepsilon_0\chi^{(2)}(\vec{r})\vec{E}(\vec{r},t)\cdot\vec{E}(\vec{r},t) = 2\varepsilon_0[d](\vec{r})\vec{E}(\vec{r},t)\cdot\vec{E}(\vec{r},t), \tag{3}$$

#261024 Received 11 Mar 2016; revised 19 Apr 2016; accepted 19 Apr 2016; published 25 Apr 2016

Table 1. Parameters of Drude-Lorentz model for Dispersive Materials.

Drude-Lorentz model	Au	MgF_2	Nanolaminate	Fused silica
ε_∞	5.9673	1.2762	1.23	1.005
ω_d (rad/s)	1.3280×10^{16}	0	0	0
γ_d (1/s)	5.7805×10^{13}	0	0	0
A_{L1}	1.0983	0.6097	1.9446	0.6940
ω_{L1} (rad/s)	4.2730×10^{15}	2.1827×10^{16}	1.0833×10^{16}	2.7761×10^{16}
γ_{L1} (1/s)	1.35×10^{15}	0	0	0
A_{L2}	0.9779	2.1497	0.4010	0.4010
ω_{L2} (rad/s)	4.9956×10^{15}	7.5398×10^{13}	1.6391×10^{16}	1.6391×10^{16}
γ_{L2} (1/s)	1.2620×10^{15}	0	0	0

where $\vec{J}_d$ is the polarization current density associated with the Drude model and $\vec{J}_{L_i}$ is the polarization current density associated with i^{th} pole of the Lorentz model, $\vec{P}^{(2)}$ is the nonlinear polarization, and [d] is the nonlinear optical coefficient tensor. The time and space derivatives in Eq. (2) are then approximated by the usual central-difference method. However, different from the linear update equations under the leap-frog scheme, the coupled nonlinear update equations require all the values of electric-field components in the future time step simultaneously. Such coupling equations are then solved by Newton iteration procedure [33, 34]. The nonlinear coefficients of the nanolaminates were set to be $\chi^{(2)}_{zzz} = 0.34\,pm/V$, $\chi^{(2)}_{xxz} = \chi^{(2)}_{yyz} = 0.36\,pm/V$, and $\chi^{(2)}_{zxx} = \chi^{(2)}_{zyy} = 0.26\,pm/V$ according to values retrieved from measurements [29]. We consider a transverse magnetic (TM) polarized light impinging from air to the system at normal incidence for all the full-wave calculations in this paper. A Gaussian-pulsed excitation is used for linear transmission spectra, and a continuous-wave excitation (E_x) with an amplitude of 0.2 V/μm is used for SHG so that the input power of the fundamental wave is 100 mW under the assumption that the source is homogeneous with a spot size of π*24.4^2 μm^2.

4. Results and discussion

4.1 Au-grating samples

Figures 2(a) and 2(b) show the transmission spectra at the fundamental wavelength and the SH wavelength, respectively, for Au-grating with w varied from 60 nm to 130 nm. For the case of TM-polarized illumination, the localized surface plasmon (LSPs) of the individual gold nanostrip is excited. The LSP hybridizes with the quasi-guided modes sustained in the nanolaminate. These eigenmodes are bound because the linear permittivity of the nanolaminate is larger than that of the substrate. The hybridized modes are known as waveguide plasmon polariton (WPP) modes [21, 35]. They exhibit a Fano line-shape as shown in the spectra in Fig. 2(b). To quantitatively study these Fano profiles, we used a fitting function consisting of the product of a symmetric Lorentzian line-shape function $\sigma_s(\nu)$ and a Fano-like asymmetric function $\sigma_a(\nu)$ [36], where $\sigma_s(\nu)$ is associated with the background plasmonic (bright) modes, and $\sigma_a(\nu)$ takes into account the interference between bright modes and waveguide (dark) modes. The fitting function is given by [36, 37],

$$\mathrm{T_{fit}}(\nu) = 1 - \sigma_a(\nu)\sigma_s(\nu) = 1 - \left[\frac{\left(\frac{\nu^2-\nu_a^2}{2\mathrm{W}_a\nu_a} + a_F\right)^2 + d}{\left(\frac{\nu^2-\nu_a^2}{2\mathrm{W}_a\nu_a}\right)^2 + 1}\right]\left[\frac{a^2}{\left(\frac{\nu^2-\nu_s^2}{2\mathrm{W}_s\nu_s}\right)+1}\right], \qquad (4)$$

where a_F is the asymmetric Fano parameter, d is the modulation damping, v_a and v_s are the central frequency of asymmetric and symmetric resonance with the spectral width W_a and W_s,

#261024 Received 11 Mar 2016; revised 19 Apr 2016; accepted 19 Apr 2016; published 25 Apr 2016

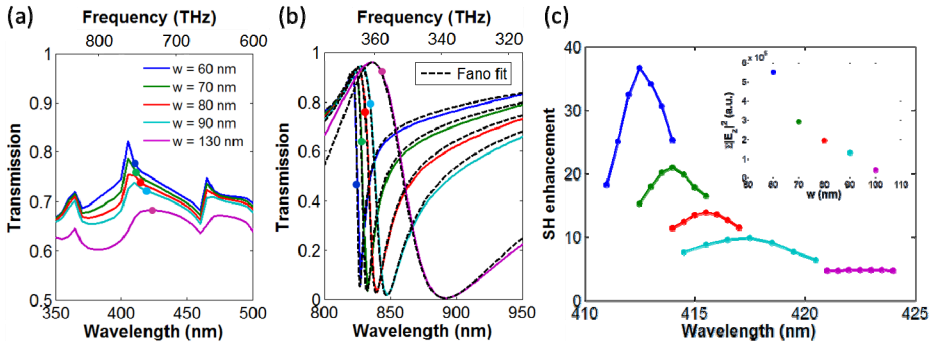

Fig. 2. Transmission spectra for Au-grating samples in the range of (a) SHG and (b) FW, respectively, where the dots point out the spectral positions of (a) the SHG emission peaks and (b) the corresponding fundamental excitations. The black-dashed curves in (b) show the Fano fits of the spectra. (c) The SH enhancement spectra for Au-grating samples with the inset showing the integration value of $|E_z|^2$ inside the nonlinear media.

respectively, and a is the maximum amplitude of the symmetric resonance. Since the asymmetric resonance dominates the spectral region we are interested in, we only list the fitting parameters v_a and W_a and the corresponding quality factor Q (i.e. $Q = v_a / W_a$) in Table 2. It can be seen that the fitted spectra [the black-dashed curves in Fig. 2(b)] are in excellent agreement with the calculation results. As w increases, the Fano resonance redshifts (v_a decreases). This is accompanied with a larger resonant bandwidth (W_a increases). Such redshift is caused by the change in the resonance wavelength of the plasmonic mode. Increasing the axis ratio simply redshifts the LSP. With an increasing strip width the radiative losses also increases, since the strip can no longer be considered as merely perturbative for the waveguide mode. These enhanced radiative losses cause the spectral broadening.

Next, the corresponding SHG for each sample is calculated with the FDTD method by integrating the SH Poynting vector in the substrate. This analysis takes fully into account how the hybrid system influences the radiation of the generated nonlinear signal. The quadratic relationship between the initial FW excitation and the SH intensity has been verified in the calculation process (not shown). Figure 2(c) shows the SH enhancement, which is defined as the SHG of the grating-coupled nanolaminates under normal incidence, $P_{SHG,0°}$, divided by the SHG of the planar nanolaminates under 45° illumination, $P_{SHG,45°}$. $P_{SHG,45°}$ is 0.017 fW as the integrating area is the same as the spot size (i.e. π*24.4^2 μm^2). No SH signal is observed for the planar nanolaminates under normal incidence due to the $C_{\infty,v}$-symmetry of the second-order susceptibility [11, 12]. It can be seen in Fig. 2(c) that as w increases the SH enhancement will decrease. One may speculate that this decline in enhancement is caused by the lower Q-factor of Fano resonance in the FW range since no higher-order resonances were excited close to the SH range [Fig. 2(a)] [38]. To prove this conjecture, we integrate the square of the electric field along the propagation direction, $\sum|E_z^{FW}|^2$, inside the nonlinear

Table 2. Parameters of the Fano line shape fitting spectra for Au-grating and MgF_2-grating samples.

Au-grating				MgF_2-grating			
w (nm)	v_a (THz)	W_a (THz)	Q	w (nm)	v_a (THz)	W_a (THz)	Q
60	363.3	1.2	315.9	80	370.34	0.042	8818
70	361.5	1.8	200.8	130	371.65	0.082	4532
80	359.4	2.9	123.9	180	373.63	0.116	3221
90	357.3	4.3	83.1	240	377.00	0.137	2752
130	351.2	12	29.3	300	380.89	0.120	3174

#261024 Received 11 Mar 2016; revised 19 Apr 2016; accepted 19 Apr 2016; published 25 Apr 2016

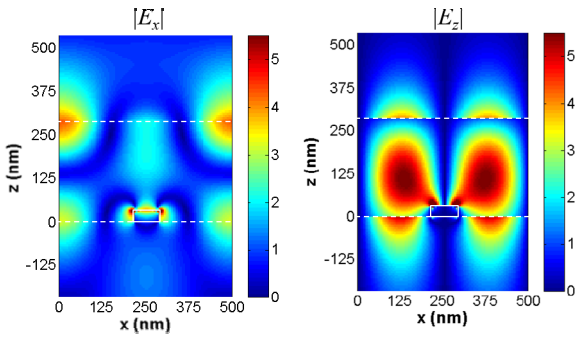

Fig. 3. Electric-field distributions at the fundamental wavelength of the SH emission peak for a Au-grating with w = 70 nm.

nanolaminates at the fundamental wavelength of each SH emission peak. This is the field component that dominantly enhances the nonlinear signal. Modal patterns with a lower amplitude were found for systems that correspond indeed to lower-Q resonances [shown in the inset of Fig. 2(c)]. This causes the reduction of the enhancement of the fundamental field as well as the SHG for samples with a larger width.

In addition, it is interesting to observe that the SHG emission peak does not occur exactly at the dip of Fano resonance. Instead, it is located in the steep slope as indicated by the dots in Fig. 2(b). Normally, the metallic loss of a resonant plasmonic structure can lead to strong energy dissipation and, hence, reduction of transmission. Due to unique coupling of LSPs andwaveguide modes in such hybrid system, the plasmonic field can be suppressed as a result of destructive interference between bright mode and quasi-guided mode [39, 40]. This is especially beneficial for the SH enhancement as the hybrid mode can provide a strong FW intensity enhancement within the nonlinear nanolaminate while avoiding the high metallic loss. Figure 3 shows the field profile for w = 70 nm at 828 nm, which corresponds to the green dot shown in Fig. 2(b). There, we can see that the WPP is strongly excited. By calculating $\sum|E_z^{FW}|^2$ at 828 nm and at the Fano transmission dip of 832 nm for w = 70 nm, we found the latter is 0.9 times lower than the former. Thus, the intensity enhancement in the nanolaminate region due to the WPP excitation is actually maximal at this slightly shifted wavelength from the Fano transmission dip, which explains why the SH signal generation is optimal there.

4.2 MgF_2-grating samples

Next, we replaced the Au-grating by a dielectric MgF_2-grating. We varied the width w from 80 nm to 300 nm. Fano resonances become extremely narrowband for such lossless structure as shown in Fig. 4(b), and meanwhile exhibit a blueshift trend as w increases. Since the permittivity of MgF_2 is smaller than that of the nanolaminate, the increase of the grating width causes the effective refractive index of quasi-guided modes to decrease, which explains the blueshift. The fitting parameters v_a and W_a and the corresponding Q-factors for all MgF_2 samples can also be found in Table 2. Different from Eq. (4), the bright mode's resonant strength was fitted here by a function of $\sigma_s(v) = gv + b$ because the background radiation is not created by a plasmonic resonance in the case of MgF_2 [36]. Instead, it corresponds only to the directly transmitted light through the layered system. The Q-factor decreases as w increases, while reaching a smallest value for w = 240 nm. One can expect the most severe perturbation when the grating width is just close to half the period. Eventually, for a width close to zero or close to the period, the radiative losses introduced by the periodic structure vanish and the Q-factor attains pretty high values. In addition, the value of $\sum|E_z^{FW}|^2$ for each SH enhancement peak, shown in the inset of Fig. 4(c), displays a good correspondence to the trend of Q-factor, which again demonstrates that the Q-factor of Fano resonance can give an

#261024 Received 11 Mar 2016; revised 19 Apr 2016; accepted 19 Apr 2016; published 25 Apr 2016

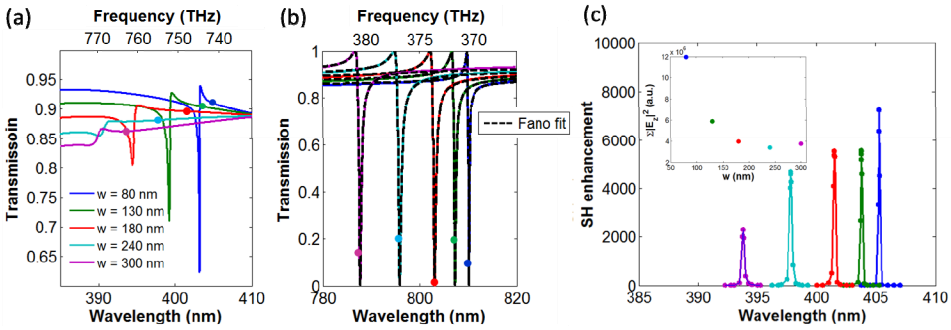

Fig. 4. Transmission spectra for MgF_2-grating samples in the range of (a) SHG and (b) FW, respectively, where the dots point out the spectral positions of (a) the SHG emission peaks and (b) the corresponding fundamental excitations. The black-dashed curves in (b) show the Fano fits of the spectra. (c) The SH enhancement spectra for MgF_2-grating samples with the inset showing the integration value of $|E_z|^2$ inside the nonlinear media.

efficient evaluation of the field enhancement in the guided layer. Therefore, as shown in Table 2, the high-Q resonance of MgF_2-grating samples are beneficial for SHG than that of Au-grating samples. However, owing to its narrowband resonance, the precision and periodicity of the gratings are of utmost importance for future experiments. Figure 4(c) shows the corresponding SH enhancement for each sample, where the enhancement reaches around 7000 for w = 80 nm. Aside from the extremely large fundamental field enhancement for the MgF_2-grating systems, higher-order Fano resonances can also be excited close to the SH wavelength region [see Fig. 4(a)]. The resonance seen in the full wave calculations for each sample corresponds to a second-order (2nd) quasi-guided mode with a two-fold standing wave profile

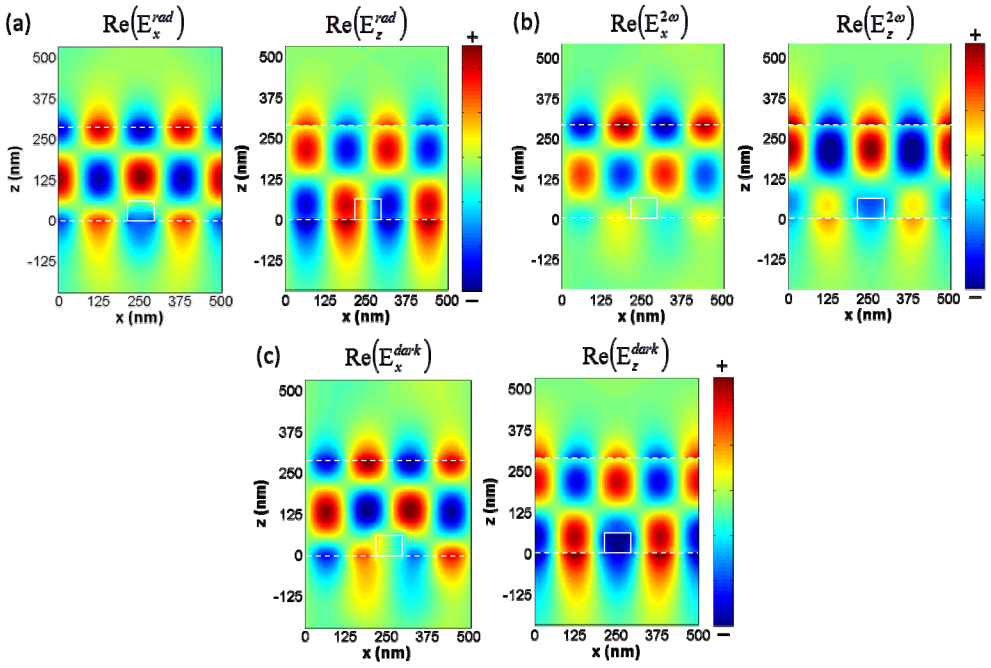

Fig. 5. Near-field distributions for (a) the 2nd quasi-guided mode, (b) the SHG emission peak of MgF2-grating with w = 80 nm, and (c) the 2nd dark waveguide mode, respectively. (a) and (b) are calculated by the FDTD program under plane wave excitation, and (c) is calculated by the eigenmode solver.

#261024 Received 11 Mar 2016; revised 19 Apr 2016; accepted 19 Apr 2016; published 25 Apr 2016

As shown in Fig. 5(a), and the Ex (Ez) field displays an even (odd) symmetry with respect to the center of the grating. Interestingly, as we examined the SH near-field [Fig. 5(b)], we found that most of the generated nonlinear signal does not couple to the bright waveguide mode [Fig. 5(a)] but rather to a dark mode, which does not interact with normal incidence or outgoing plane waves. Eigenmode calculations using the finite-element solver JCMsuite [41] reveal that the dark mode field profile [Fig. 5(c)] overlaps well with the SH near field. Thus, a significant portion of the SHG remains guided in the nanolaminates and is forbidden to radiate to the far-field because of the odd parity of Ex-field [42]. Such property can be potentially exploited as a nonlinear light source in on-chip photonic platforms.

4. Conclusion

In conclusion, we have demonstrated the SH emission can be significantly enhanced by introducing gratings to a nonlinear nanolaminate waveguide layer. The degree of enhancement depends on the *Q*-factor of the Fano resonance. The emission peak occurs where a strong field is excited in the guided layer rather than at the dip of Fano resonance. The SH emission reaches an enhancement of 38-fold and 7000-fold enhancement for Au-grating (w = 60 nm) and MgF_2-grating (w = 80 nm), respectively. In addition, for the MgF_2-grating samples, the generated SH signal was found to be strongly coupled to the dark mode and remain guided in the nanolaminate layer.

Acknowledgments

We thank the financial support by Ministry of Science and Technology of Taiwan under Grant NSC 104-2917-I-564-083. Funding by the Deutsche Forschungsgemeinschaft (DFG SPP 1391 Ultrafast Nanooptics) within project RO 3640/2-2 is also acknowledged as well as by the Helmholtz International Research School for Teratronics (HIRST) and the Karlsruhe School of Optics & Photonics (KSOP). We also acknowledge support by the Deutsche Forschungsgemeinschaft and Open Access Publishing Fund of Karlsruhe Institute of Technology.

#261024 Received 11 Mar 2016; revised 19 Apr 2016; accepted 19 Apr 2016; published 25 Apr 2016